Contact stresses for multiply-connected Regions - the case of pitted spheres*

K. P. Singh, B. Paul and W. S. Woodward

NOMENCLATURE

A_{ij}	area of cell i, j
a_{ij}	coefficient in eq. (21)
B_{ij}	coefficient in eq. (23)
c_{ijl}	distance between field point l and a point in cell S_{ij}
$\bar{c}_{ijl}$	distance between field point l and centroid of cell S_{ij}
d	hypothetical interpenetration
d_0	initial interpenetration of spheres
e'	separation (gap) between corresponding surface points after load is applied
E	Young's modulus
$f(x, y)$ or $f(r)$	initial separation between surface points
f_i	$f(r)$ evaluated at field point i
f'_i	$f_{N+1} - f_i$
F	normal load
F^*	dimensionless normal load, $kF/(R)^2$
I_{ijl}	$\int_{S_{ij}} \mathrm{d}A_{ij}/c_{ijl}$
k	elastic parameter
m	number of equal sectors in Ω
n	number of cells in Ω
N	number of annular rings in Ω
N_{con}	number of cells within radius r_{con}
$p(x, y)$	interfacial contact pressure
p_i	piecewise constant pressure in annular ring i
p_i^*	dimensionless pressure, kp_i
r	radius defined from origin of Ω
r_b	radius of blending point of pit and sphere

* This research was partially supported by the Federal Railroad Administration of the U.S. Department of Transportation under Grant DOT-05-40093.

r_c	radius of curvature at 'edge' of pit
r_{con}	radius used in convergence studies
r_i	inner radius of contact region
r_0	outer radius of contact region
$r\Delta\phi$	width of cell
Δr	length of cell
r^*	r/R
r_b^*	r_b/R
r_c^*	r_c/R
R	effective radius $(2R_1R_2)/(R_1+R_2)$
R_1	radius of sphere with pit
R_2	radius of smooth sphere
S_{ij}	region included in ring i between rays j and $j+1$
SCF	stress concentration factor
v_j	vector in eq. (22)
x'	radius of point 0′ in Fig. 2
(x, y)	Cartesian coordinates in the fixed reference plane
α	$\Delta\phi/2$ half-angle of sector
β_{ij}	centroidal radius of sector S_{ij}
δ	relative approach
δ^*	δ/R
θ	semi-vertex angle (Fig. 1)
ν_1, ν_2	Poisson's ratio of bodies 1 and 2 respectively
ξ_i	inner radius of ring i
ρ	a boundary radius (r_i or r_0) of the contact region
ϕ	polar coordinate in fixed reference plane
$\Delta\phi$	$2\pi/m$
Ω	region of contact
Ω_i	region of cell i
Ω^*	candidate contact region.

1. INTRODUCTION

Contact problems involving multiply-connected contact regions have received little attention in the literature, possibly because of the non-Hertzian nature of such problems. Such problems arise, for example, whenever either of the contacting bodies have surface pits (e.g. casting defects, corrosion pits, machining faults, etc.). Barely perceptible surface flaws can cause high stress concentrations, and consequently, rapid fatigue failure. Experimental observations by Tallian[1], Martin and Eberhardt[2] and Littman and Widmer[3] indicate that such surface defects may be potential nuclei of microcrack propagation and can produce rapid destruction of rolling surfaces.

Based on the degree of difficulty associated with their solution, these

problems may be divided into the following two categories:

i. Contact region known *a priori*:
When the indentor contact surface is flat (or almost flat) it will be called a 'stamp', and the contact surface is defined *a priori* by the stamp boundary. When the indentor surface is not flat, but the indentor has a substantially higher elastic modulus than the indented body, the indentor can be treated as rigid, and the shape of the contact region becomes known for any given depth of penetration relative to the indentor tip.

ii. Elastic contact problems:
When the indentor is not a stamp, and the two bodies have comparable elastic moduli, then the geometry of the contact region is unknown *a priori*, and it must be determined by solving the appropriate elasticity problem.

To the best of our knowledge, no solutions to problems of category (ii), for three-dimensional elastostatics with multiply-connected regions, have been reported in the literature. However, solution of a few special cases of rigid indentor problems (category (i)) have been found by Olesiak[4], Parlas and Michalopoulos[5] and Chiu[6].

Olesiak[4] solved the problem of an annular flat faced-stamp pressed on an elastic half space. Parlas, et al. proposed the solution for a 'bolt shaped' indentor pressed into an elastic half-space with a cylindrical hole. The cylindrical (bolt) section of the indentor was assumed to be rigidly bonded to the wall of the cylindrical hole while the bottom face of the bolt head presses against the half-space.

Chiu[6] solved the problem of an infinitely long rigid cylinder in contact with an elastic half-space, where the rigid cylinder has a groove running parallel to its axis.

In this paper, we give results which indicate that problems of both categories (i) and (ii) may be successfully solved by an extension of the method introduced by Singh and Paul[7].

A brief synopsis of the simply-discretized method of solution is given in Section 2, and some limitations and advantages of this method are discussed in Section 3. The example problem of a pitted sphere in contact with a complete sphere is described in Section 4. Techniques devised for an accurate numerical solution and rapid convergence are described in Section 5. Results for an example are given in Section 6, and conclusions are reviewed in Section 7.

2. THE SIMPLY DISCRETIZED METHOD OF SOLUTION

Singh and Paul[7] proposed a group of numerical methods for the solution of frictionless elastic contact problems where the surface profiles of the

contacting bodies are allowed to have discontinuities in slope and curvature. One of their solution procedures, called the 'simply discretized method', is briefly recapitulated in this section. For a detailed description of the theoretical foundation and applicability of the method, the reader is referred to Singh[8] or Singh and Paul[9].

We will restrict our attention to 'nonconformal' contact problems where the dimensions of the contact region are small compared to appropriate radii of curvature of the undeformed bodies. Therefore, we may assume that the contact surfaces do not deviate significantly from a reference plane in which we imbed fixed Cartesian axes (x, y). Furthermore, we shall consider only those cases where the two bodies undergo a relative rigid body translation of amount δ, in a direction normal to the reference plane, plus an elastic deformation. The translation δ is called the 'relative approach' and is positive if it moves the bodies towards one another. We will also assume that the applied load consists of a force F, acting normal to the reference plane, and that the contacting surfaces have a sufficient degree of symmetry that the resultant of the contact pressures on each body is a force of magnitude F which acts through the origin 0 of the reference plane and equilibrates the applied force F.

It is well known (see for example Luré[10]) that the fundamental integral equation for nonconformal contact stress problems is

$$k \int_{\Omega} \frac{p(x', y')\, dx'\, dy'}{[(x-x')^2 + (y-y')^2]^{1/2}} - \delta + f(x, y) = e'(x, y) \tag{1}$$

where the 'elastic parameter' k is defined as

$$k = \frac{1-\nu_1^2}{\pi E_1} + \frac{1-\nu_2^2}{\pi E_2} \tag{2}$$

In the foregoing equations, ν_1, ν_2 and E_1, E_2 denote the Poisson's ratio and Young's modulus respectively for body 1 (indentor) and body 2 (indented); $p(x', y')$ is the normal pressure over the contact surface; Ω is the projection of the contact surface on the (x, y) reference plane; $f(x, y)$ represents the initial separation (or gap) between surface points on the two bodies, located at the same (x, y) coordinates, before the load F is applied; $e'(x, y)$ is the separation of the opposed surface points after the load is applied. Fig. 1 illustrates the initial separation f for a case of axial symmetry where f is a function $f(r)$ of the radial coordinate r.

The condition of impenetrability of matter requires that $e'(x, y)$ should vanish inside Ω and it should be positive outside of Ω. Conversely, the interfacial contact pressure $p(x, y)$ should be positive inside Ω, and it should vanish identically outside of it. In symbolic terms,

$$e' = 0 \qquad \text{for} \quad (x, y) \text{ inside } \Omega \tag{3a}$$

$$e' > 0 \qquad \text{for} \quad (x, y) \text{ outside of } \Omega \tag{3b}$$

$$p(x, y) = 0 \quad \text{for} \quad (x, y) \text{ outside of } \Omega \tag{4a}$$

$$p(x, y) \geq 0 \quad \text{for} \quad (x, y) \text{ inside } \Omega \tag{4b}$$

In short, a solution of the problem requires the determination of the boundaries of region Ω, a pressure field $p(x, y)$, and an approach δ which

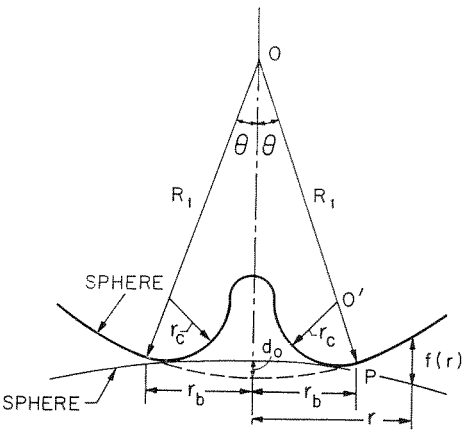

Fig. 1. Geometry of pitted surface; $f(r)$ is initial separation

satisfy relations (1)–(4). The associated load may be found from the expression

$$F = \int_{\Omega} p(x, y)\, \mathrm{d}x\mathrm{d}y$$

The absence of foreknowledge of the contact region Ω is a major impediment to a mathematical solution. This obstacle is overcome by postulating a tentative contact region Ω^*. Singh and Paul[7] proposed that the 'interpenetration curve' described by

$$f(x, y) = d \tag{5}$$

be used as a tentative contact region. Equation (5) defines the contour of the curve formed by interpenetration (without deformation) of the two surfaces through an arbitrary distance d. Picking a suitable value of d establishes the candidate contact region Ω^*. Using this as a preliminary estimate of Ω, equation (1) is readily recognized to be an integral equation of the first kind. A 'simply discretized' numerical solution of equation (1) is found by subdividing Ω into a large number of small cells. The pressure function $p(x, y)$ is replaced by a piecewise constant pressure field (pressure p_i

in cell i). Thus if Ω is subdivided into n cells, equation (1) becomes

$$\sum_{i=1}^{n} kp_i \int_{\Omega_i} \frac{dx'\,dy'}{[(x-x')^2+(y-y')^2]^{1/2}} - \delta + f(x,y) = e' \tag{6}$$

where Ω_i is the region of cell i. In equation (6), n values of p_i and the constant δ are unknowns to be determined. The centroids (x_i, y_i) of the cells are taken as field points (x, y) and equation (6) is written for each field point. The integrals in equation (6) are evaluated by numerical quadrature. Thus n linear algebraic equations are generated. An additional independent linear equation, essential for a unique solution, is generated by picking up a field point other than the cell centroids. The choice of this additional field point is otherwise arbitrary, however, it does affect the quality of the results, as discussed in Section 4.

Having thus generated a set of $n+1$ linear equations, the n unknown pressures, p_i, and the approach δ, are obtained through Gaussian elimination. The next step in the solution is to determine whether the tentatively selected region of integration Ω^* is indeed the true contact region. This is done by utilizing the inequalities (3) and (4), and systematically adjusting the boundaries of Ω until these inequalities are satisfied.

3. LIMITATIONS AND ADVANTAGES OF THE SIMPLY-DISCRETIZED METHOD

Singh and Paul[7] showed that the simply-discretized method just described is numerically unstable in the general case. This is due to the fact that the solution vector of the set of linear algebraic equations generated is very sensitive to small perturbations in elements of the coefficient matrix. Since such perturbations are unavoidable in the discretization process, the solution vector tends to be very erratic. Large oscillations in the solution vector correspond to small perturbations in the elements of the coefficient matrix. This behavior is similar to that observed in ill-posed problems of partial differential equations, as discussed by Hadamard[11]. For problems which do not show axisymmetry (or where axisymmetry is not utilized), Singh and Paul[7] found that the simply discretized method was incapable of predicting the proper stress distribution. For such problems they found it necessary to introduce stabilizing techniques known as the 'redundant field point method', and the 'functional regularization method' (see [7,9]).

The amount of numerical computation required for either of the two last named methods exceeds that of the simply discretized method. Accordingly, it is desirable to use the latter whenever circumstances permit.

In this paper we will focus on a problem with complete axisymmetry, and it will be shown that the simply discretized method provides an excellent solution, provided that the maximum possible use is made of the symmetry of the problem.

In other words, we recognize that all cells located at the same radius from the axis of symmetry have the same contact pressure at their centroids, and the number of unknown pressures p_i is reduced from n (the number of cells) to N (the number of annular rings formed by an axisymmetric distribution of cells). By using the simply discretized method, we are able to utilize inequality (4b) to iteratively refine the region of contact Ω. Upon satisfying inequality (4b), it was invariably found that inequality (3b) was satisfied.

The nature of the functional regularization method prohibits the use of inequality (4b) as a basis for refining Ω.

Numerical experiments have indicated that iteration procedures based up on inequality (4b) converge much faster than those based upon inequality (3b). Further details of the iteration procedures will be found in Sections 5 and 6.

4. PITTED SPHERE GEOMETRY

As a typical example, contact of a pitted elastic sphere of radius R_1 with an unpitted elastic sphere of radius R_2 is considered. A section of the pitted surface by a plane through the axis of symmetry is shown in Fig. 1. The local contour of the pitted surface is idealized as a torus smoothly blended into a sphere. The blending point P, where the pit joins the main surface, is located at a distance r_b from the load line. The center of curvature $0'$ of the pit blending arc lies on the conical surface of semi-vertex angle θ. The meridional radius of curvature of the torus is r_c.

Note that the discontinuity in curvature which occurs at P does not preclude the use of the method of solution described. A tentative contact

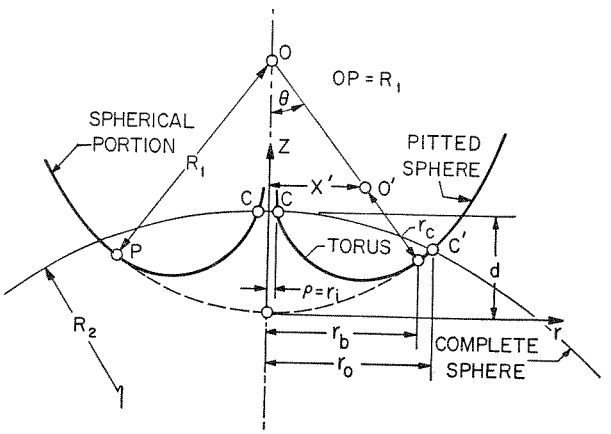

Fig. 2. Generation of annular interpenetration region

region, Ω, is established by a hypothetical interpenetration of the two spheres through a distance d. The annulus of contact so formed is bounded by an inner radius r_i and an outer radius r_0 as shown in Fig. 2, where suitable coordinate axes r, and z are indicated. The values of r_i and r_0 for a given problem are determined as follows. The z coordinate of a point $C(\rho, z_1)$ located at a distance ρ from the z-axis on the portion of body 1 (see Fig. 2), where

$$\rho < r_b, \tag{7a}$$

is:

$$z_1 = R_1 - (R_1 - r_c)\cos\theta - [r_c^2 - (x' - \rho)^2]^{1/2} \tag{7b}$$

where

$$x' = \frac{(R_1 - r_c)\, r_b}{R_1} \tag{7c}$$

$$\theta = \sin^{-1}\frac{r_b}{R_1} \tag{8}$$

The z-coordinate of a point on sphere 2, located at a distance ρ from the z-axis, is given by

$$z_2 = d - [R_2 - (R_2^2 - \rho^2)^{1/2}] \tag{9}$$

Since point C lies on both the torus and the lower sphere, $z_1 = z_2$; thus equations (7b) and (9) require that

$$d = R_1 - (R_1 - r_c)\cos\theta - [r_c^2 - (\rho - x')^2]^{1/2} + R_2 - (R_2^2 - \rho^2)^{1/2} \tag{10}$$

$$\rho < r_b \tag{10a}$$

Furthermore, the z-coordinate of a material point C' located on the spherical portion of body 1, at a distance ρ from the z-axis, is given by

$$z_1 = R_1 - (R_1^2 - \rho^2)^{1/2} \tag{11}$$

where

$$(\rho > r_b) \tag{11a}$$

Hence, for a given interpenetration d, the radius ρ of a point on the intersection of sphere 2 and spherical region of body 1 is given by

$$d = R_1 - (R_1^2 - \rho^2)^{1/2} + R_2 - (R_2^2 - \rho^2)^{1/2} \tag{12a}$$

$$(\rho > r_b) \tag{12b}$$

The geometry of the toroidal surface indicates that for $r_c < R_1$, equation (10) has two solutions for ρ. Let ρ_1 and ρ_2 $(\rho_1 < \rho_2)$ be roots of equation (10). Two cases are readily identified.

Case i. When both inner and outer radii of the assumed contact region lie inside the blending radius, i.e.

$$\rho_2 < r_b \tag{13}$$

In this case the contact is assumed to be completely confined to the toroidal segment of body 1, in which case

$$\begin{aligned} r_i &= \rho_1 \\ r_0 &= \rho_2 \end{aligned} \tag{14}$$

Case ii. When the outer boundary of Ω lies beyond the blending radius (as shown in Fig. 2), i.e.

$$\rho_2 > r_b \tag{15}$$

In this case

$$r_i = \rho_1$$

and the outer radius r_0 is determined from the solution of equation (12). Note that equations (10) and (12) are transcendental in ρ, which can be found by an iterative procedure (e.g. Newton-Raphson).

In order to find the initial separation $f(r)$, shown in Fig. 1, it is only necessary to find

$$f(r) = z_1 - z_2 \tag{15a}$$

where z_2 is found from equation (9) with $\rho \equiv r$ and $d \equiv d_0$; d_0 is the value of d corresponding to initial contact as shown in Fig. 1. To find z_1, set $\rho \equiv r$ and use equation (7b) for points on the torus ($r < r_b$), or equation (11) for points on the upper sphere ($r > r_b$).

In order to find the initial separation d_0, it is necessary to note from Fig. 1, that when $d = d_0$, the slope of the torus matches that of the lower sphere at the contact point; i.e.

$$\frac{\mathrm{d}z_1}{\mathrm{d}\rho} = \frac{\mathrm{d}z_2}{\mathrm{d}\rho} \tag{15b}$$

where the derivatives are found from equation (7b) and equation (9). Equation (15b), together with equations (7b) and (9), suffice to find d_0, and the two coordinates (r, z) of the initial contact point.

Having found the boundaries (r_i and r_0) of the contact region Ω and the initial separation function $f(r)$, we may proceed to solve the governing integral equation (1).

5. NUMERICAL SOLUTION PROCEDURE

The contact region Ω is subdivided into N annular rings. Since a steep pressure gradient is expected near the pit, the annular rings near the inner boundary are very narrow in width. It was also learned from experience that the peak pressure always occurs at some radius r where $r < r_b$. Guided by this consideration, a majority of the rings are clustered in the region $r_i \leq r \leq r_b$. Exploiting the axisymmetry of the problem, we assume that the pressure is constant in each ring. The rings are numbered sequentially from 1 to N, from the inside out, and the pressure in the i-th ring is assumed to be an unknown constant p_i. Let ξ_i and ξ_{i+1} be the inner and outer bounding radii for cell i; thus $\xi_1 \equiv r_i$ and $\xi_{N+1} \equiv r_0$. Each ring is further subdivided circumferentially into m equal sectors by drawing (m) equispaced radial rays from the center of Ω; the angle $\Delta\phi$ between two adjacent rays is $2\pi/m$. The sector, bounded by radial rays 1 and 2, is shown in Fig. 3.

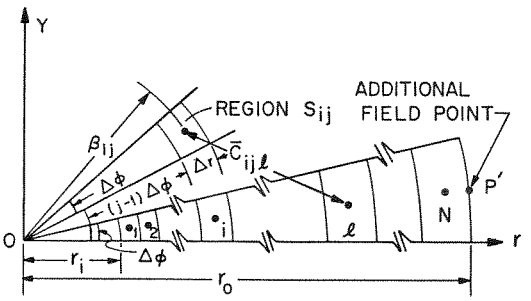

Fig. 3. Subdivided and labeled contact region (portion)

The region of the sector located in the i-th ring, between ray j and ray $(j+1)$, is identified as S_{ij}; and its centroidal radius by β_{ij}. Elementary calculations show that

$$\beta_{ij} = \frac{2\sin\alpha}{3\alpha} \frac{(\xi_{i+1}^2 + \xi_i^2 + \xi_{i+1}\xi_i)}{(\xi_{i+1} + \xi_i)} \tag{16}$$

where

$$\alpha = \pi/m = \Delta\phi/2 \tag{17}$$

The centroids of the first sector shown in Fig. 3 (i.e. where $j = 1$) are selected as field points.

Thus for the field point l, equations (6) and (3a) reduce to

$$k \sum_{i=1}^{N} p_i \sum_{j=1}^{m} \int_{S_{ij}} \frac{dA_{ij}}{c_{ijl}} - \delta + f(\beta_{l1}) = 0 \tag{18}$$

where $f(r)$ is calculated for $r = \beta_{ll}$ from equation (15a). c_{ijl} is the radial distance from field point l to the elemental area dA_{ij} located in S_{ij}. For most cells, the integral in equation (18) may be replaced by the approximation

$$I_{ijl} = \int_{S_{ij}} \frac{dA_{ij}}{c_{ijl}} = \frac{A_{ij}}{\bar{c}_{ijl}} \tag{19}$$

where $\bar{c}_{ij}$ is the distance between field point l and the centroid of the region S_{ij}, whose area is denoted by A_{ij}. It was shown in Singh[8] that, in general, equation (19) is a very useful approximation which results in a significant reduction of computation time, without compromising the accuracy of results. However, for regions located in the immediate vicinity of the field point l, the errors due to the approximation (19) may be unacceptable. To avoid such errors, I_{ijl} is evaluated by numerical quadrature within cells located near the field point. The criterion which must be satisfied in order to use equation (19) is

$$\bar{c}_{ijl} > \max[r\Delta\phi, \Delta r] \tag{20}$$

In equation (20), $r\Delta\phi$ and Δr are the side lengths of a typical cell. Notice that when the field point l lies inside the region S_{ij} (i.e. $j = 1$, $i = l$), $\bar{c}_{ijl} = 0$, and hence the integrand in equation (14) has a singularity. However, for such cases, an approximate analytical solution for the integral is readily constructed.

In this manner, N linear equations corresponding to the N field points are generated. An additional linearly independent equation is generated by selecting point P' at the outermost boundary of the contact region as field point $(N+1)$. The location of this additional field point has a pronounced affect on the solution, which deteriorates as P' is moved inside the boundary. It is plausible to assume that this behavior is due to the gradual increase in cell width Δr with r (see Fig. 3), which was introduced to keep the aspect ratio of the cells from becoming excessive. With the cells so designed, the location of P' shown in Fig. 3 maximizes the distance between P' and its nearest neighboring field point. This in turn tends to maximize the amount of independent information supplied by the equation written for field point P', and should tend to minimize ill-conditioning effects on the coefficient matrix generated.

Thus $(N+1)$ equations in $(N+1)$ unknowns are generated, and equation (18) assumes the form

$$a_{ij} p_j = -f_i + \delta \tag{21}$$

and the equation constructed using P' as a field point becomes,

$$v_j p_j = -f_{N+1} + \delta \tag{22}$$

where f_i is the value of the 'initial separation' function $f(r)$ at the field point i. f_{N+1} is the value of $f(r)$ at P'; and summation from 1 to N is

henceforth implied over repeated subscripts. From equations (21) and (22), δ may be eliminated to yield

$$B_{ij}p_j = f_i' \tag{23}$$

where

$$B_{ij} = A_{ij} - v_j \tag{24}$$

and

$$f_i' = f_{N+1} - f_i \tag{25}$$

When equation (23) is solved for p_i, using Gaussian elimination, the resulting pressure distribution is usually found to predict negative contact pressures in the immediate vicinity of the inside boundary, $r = r_i$. The axisymmetry of the problems enables us to maintain the outside boundary fixed, and iterate on the inside boundary where the predicted pressure is incorrect. The iteration scheme is best explained with the aid of the numerical example given in Section 6.

6. A NUMERICAL EXAMPLE

The following example was considered.

$R_1 = R_2 = 1$ in.

$v_1 = v_2 = 0.$

$E_1 = E_2 = 30 \times 10^6$ b/in^2

$r_c = .006$ in

$r_b = .00025$ in.

The results are presented in dimensionless form. Let

$$R = \frac{2R_1R_2}{R_1 + R_2} \tag{26}$$

Then, we define

Dimensionless pressure in ring i, $p_i^* = kp_1$ (27)

Dimensionless load, $F^* = \dfrac{kF}{R^2}$ (28)

Dimensionless distance from origin of Ω, $r^* = r/R$ (29a)

Dimensionless approach, $\delta^* = \delta/R$ (29b)

$r_b^* = r_b/R$ (30a)

$r_c^* = r_c/R$ (30b)

Fig. 4 shows the pressure distribution near the inside boundary for the uniterated solution. The pressure distribution far from the pit agrees closely

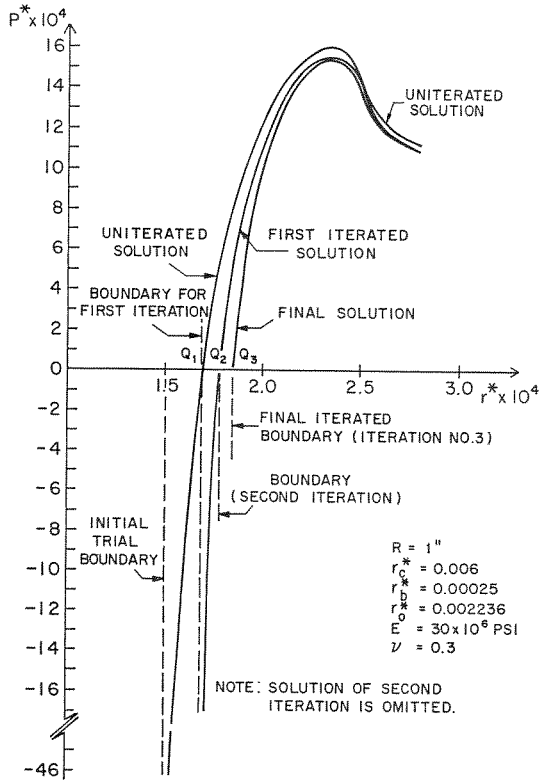

Fig. 4. Boundary iteration sequence

with the Hertzian solution for unpitted spheres (not shown in the figure). However, the pressure in cell # 1 is highly negative. The pressures in the successive cells are less and less negative, until at point Q_1 the pressure curve crosses the x-axis. The shape of the pressure curve readily suggests the iteration scheme. The new region of integration is assumed to have inner radius $r_i = 0Q_1$. The discretized equation set (23) is generated corresponding to this new region Ω, and thus a new pressure vector is generated (see first iteration, Fig. 4). This new curve also has a negative peak (weaker than that of the uniterated solution) at the innermost field point. The new point of intersection is Q_2, which defines the inner boundary of Ω for the next iteration. The process is thus continued until all pressures are positive. In Fig. 4, the third iteration yields the desired solution. It is found that this solution also satisfies inequality (3), thus qualifying as the

'true' solution of the contact problem. The complete pressure distribution is shown in Fig. 5. Notice the essentially Hertzian pressure distribution (corresponding to contact of unpitted spheres) at $r^* > 6 \times 10^{-4}$. Thus the

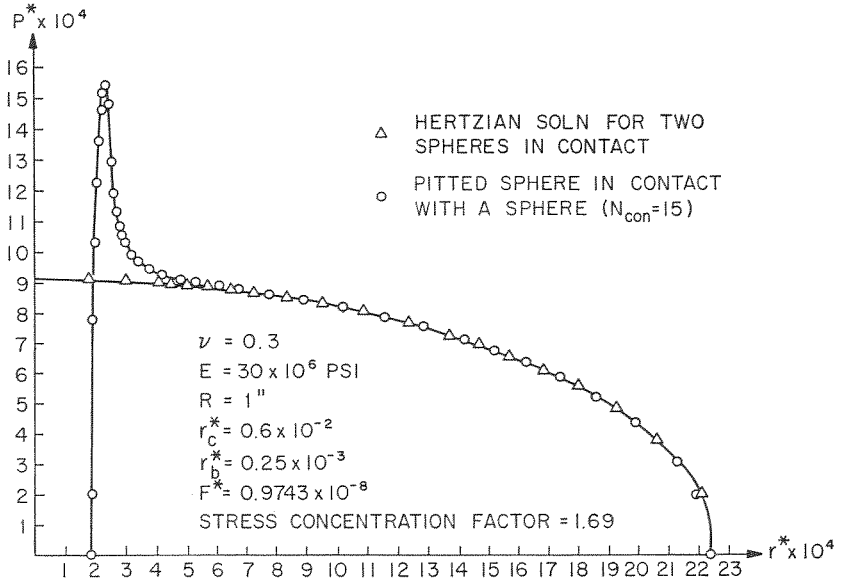

Fig. 5. Pressure distribution for pitted sphere pressed against a sphere

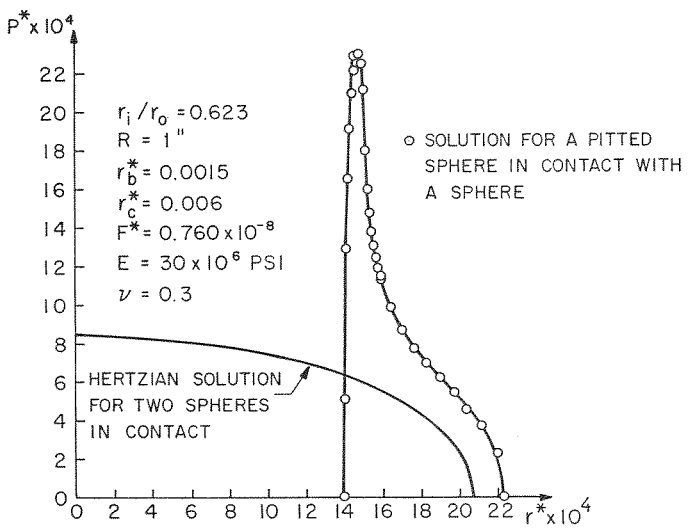

Fig. 6. Pressure distribution for large pit diameter

effect of the cavity is of a strictly localized nature. However, as the cavity is made larger (e.g. $r_i/r_0 \geq 0.3$) the pressure curve departs completely from the Hertzian case. For example, Fig. 6 shows a typical pressure distribution for $r_i/r_0 = 0.623$, along with the Hertzian solution for unpitted spheres corresponding to identical values of thrust F.

In order to establish confidence in the solution, it is necessary to study its convergence with change in the number of cells used. It must be recognized that it is necessary for the cells to be densely concentrated only in that region where a high pressure gradient exists. Therefore, for purposes of convergence studies, we have systematically varied the number of cells

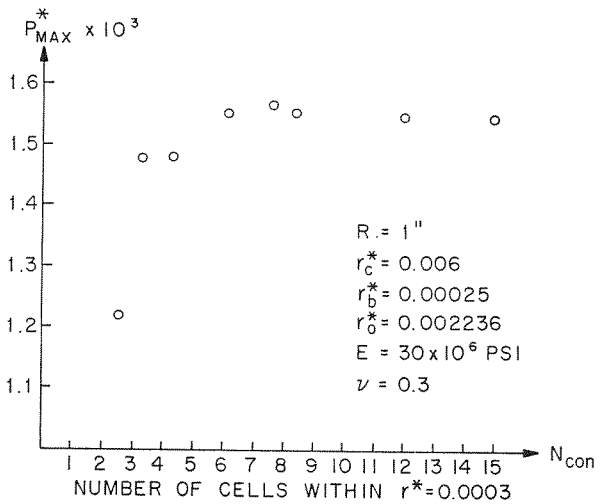

Fig. 7. Convergence of peak pressure with increasing number of cells

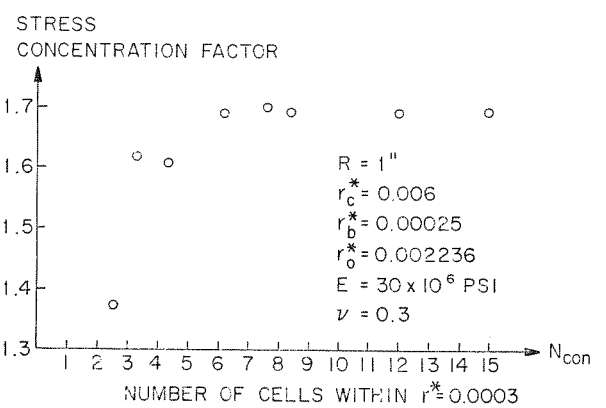

Fig. 8. Convergence of stress concentration with increasing number of cells

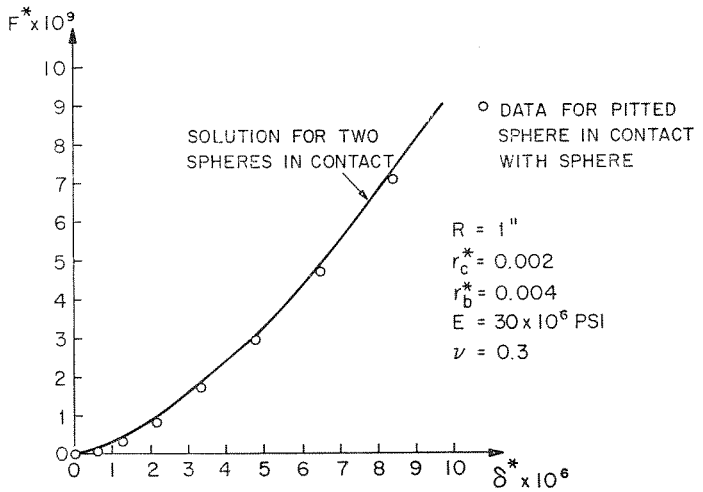

Fig. 9. Load approach relationship

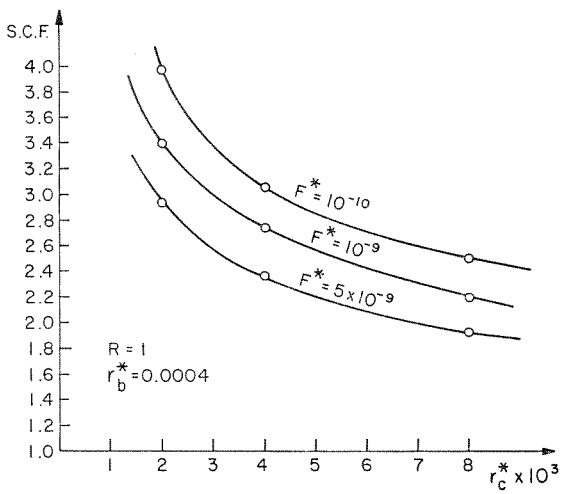

Fig. 10. The effect of load and r_c on stress concentration factor

within a fixed radius r_{con}. This radius is chosen arbitrarily for each problem in such a way that the major area of stress concentration lies inside the radius r_{con}. For the example problem considered, $r_{con} = .0003$. Let N_{con} be the number of rings located within radius r_{con}. Fig. 7 illustrates the convergence of the peak pressure, p^*_{max}. Fig. 8 shows the convergence of stress concentration factor with N_{con}. Stress concentration factor (SCF) is

defined as the ratio of the peak computed pressure to the peak pressure for unpitted spheres under equal thrust. Notice both Figs. 7 and 8 exhibit convergence for $N_{con} > 8$.

The load-approach curve is shown in Fig. 9. It is obvious from Fig. 9 that the compliance characteristics of the balls (with small pits) remain essentially the same as that predicted by the Hertzian solution.

Fig. 10 shows SCF as a function of cavity edge radius r_c^*. Smaller values of r^* cause greater stress concentration. Due to the nonlinearity of the problem, the SCF is also a function of the applied load F_c^*. Table 1 shows

Table 1. Dependence of stress concentration factor on r_b

Case No.	$r_b^* \times 10^3$	*SCF*	$F^* \times 10^8$	$\delta \times 10^4$	$r_l^* \times 10^3$
1	0.25	1.692	0.9743	0.1023	0.1845
2	0.35	1.856	0.9737	0.1029	0.2753
3	0.50	2.049	0.9702	0.1041	0.4166

$R = 1''$, $r_c^* = 0.006$, $r_0^* = 0.002236$, $E = 30 \times 10^6$ *psi*, $\nu = 0.3$

the variation of SCF with the size of the pit (measured by blend point radius). Notice the SCF increases with increasing value of r_b^*. This variation of SCF with r_b^* may be related to the loss of load carrying area.

The computer program developed to solve this problem is moderately efficient. For example, the nine cases, needed to generate Fig. 10, required an average running time of 10 minutes each on the IBM/360/65 computer, corresponding to \$8.33 per case, with $N = 34$ nodes per case.

7. CONCLUSIONS

A non-Hertzian elastic contact problem involving an unknown multiply-connected contact region has been solved. The example problem considered is that of a pitted sphere in contact with an unpitted sphere. The axi-symmetry of the problem enabled us to use the 'simply-discretized method' with a polar coordinate grid. For problems with a lower degree of symmetry, it had been found in earlier work, that a more complicated (and less efficient) method of solution was necessary because of the numerical instability of the equations generated. It may be appropriate to describe the equation set (23) as 'quasi-stable' because it exhibits dependence on the location of the $(N+1)$th field point. Through experience and heuristic reasoning, it was established that locating the additional field point (P' in Fig. 3) at the outside boundary yields a well-conditioned matrix.

The variation of the SCF, contact region Ω and peak pressure p_{max}^* with

changes in the pit blending radius r_b^*, and the pit edge radius r_c^*, was studied, and some numerical results were presented.

The numerical solution was shown to converge rapidly with a moderate cell density.

To the best of our knowledge, this is the first published solution of a multiply-connected contact region problem with *a priori* unknown contact boundary.

REFERENCES

1. T.E. Tallian, 'On Competing Failure Modes in Rolling Contact', *ASLE Trans.*, **10**, 4, 1967, pp. 418–435.
2. J.A. Martin and A.D. Eberhardt, 'Identification of Potential Failure Nuclei in Rolling Contact Fatigue', *J. of Basic Engrg., Trans. of the ASME*, D, **80**, 1967, pp. 932–942.
3. W.E. Littman and R.L. Widmer, 'Propagation of Contact Fatigue from Surface and Subsurface Origin', *J. of Basic Engrg., Trans. of the ASME*, D, **88**, 1966, pp. 624–636.
4. Z. Olesiak, 'Annular Punch on Elastic Semi-Space', *Archwm. Mech. Stosow*, **17**, 4, 1965, pp. 633–642.
5. S.C. Parlas and C.D. Michalopoulos, 'Axisymmetric Contact Problem for an Elastic Half-Space with a Cylindrical Hole', *Int. J. of Engrg. Sc.*, **10**, 1972, pp. 699–707.
6. Y.P. Chiu, 'On the Contact Problem of Cylinders Containing a Shallow Longitudinal Surface Depression', *J. of Appl. Mech.*, **36**, *Trans. of the ASME*, **91**, Series E, 4, 1969, pp. 852–858.
7. K.P. Singh and B. Paul, 'Numerical Solution of Non-Hertzian Elastic Contact Problems', *J. of Appl. Mech.*, **41**, *Trans. of the ASME*, **96**, Series E, 2, 1974, pp. 484–496.
8. K.P. Singh, *Contact Stresses in Elastic Bodies with Arbitrary Profiles*, Ph. D. thesis, University of Pennsylvania, 1972.
9. K.P. Singh and B. Paul, 'A Method for Solving Ill-Posed Integral Equations of the First Kind', *Computer Methods in Applied Mechanics and Engineering*, **2**, 1973, pp. 339–348.
10. A.I. Luré, *Three Dimensional Problems of the Theory of Elasticity*, Interscience, 1964.
11. J. Hadamard, *Lectures on Cauchy's Problem in Linear Partial Differential Equations*, Dover Publications, New York, 1952, pp. 33–34.